Rheol Acta (2012) 51:579–593
DOI 10.1007/s00397-012-0632-z

ORIGINAL CONTRIBUTION

Magnetorheology in an aging, yield stress matrix fluid

Jason P. Rich · Patrick S. Doyle · Gareth H. McKinley

Received: 7 November 2011 / Revised: 16 April 2012 / Accepted: 17 April 2012 / Published online: 8 May 2012

Abstract Field-induced static and dynamic yield stresses are explored for magnetorheological (MR) suspensions in an aging, yield stress matrix fluid composed of an aqueous dispersion of Laponite® clay. Using a custom-built magnetorheometry fixture, the MR response is studied for magnetic field strengths up to 1 T and magnetic particle concentrations up to 30 v%. The yield stress of the matrix fluid, which serves to inhibit sedimentation of dispersed carbonyl iron magnetic microparticles, is found to have a negligible effect on the field-induced static yield stress for sufficient applied fields, and good agreement is observed between field-induced static and dynamic yield stresses for all but the lowest field strengths and particle concentrations. These results, which generally imply a dominance of interparticle dipolar interactions over the matrix fluid yield stress, are analyzed by considering a dimensionless magnetic yield parameter that quantifies the balance of stresses on particles. By characterizing the applied magnetic field in terms of the average particle magnetization, a rheological master curve is generated for the field-induced static yield stress that indicates a concentration–magnetization superposition. The results presented herein will provide guidance to formulators of MR fluids and designers of MR devices who require a field-induced static yield stress and a dispersion that is essentially indefinitely stable to sedimentation.

Keywords Magnetorheology · Yield stress · Aging · Clay · Suspensions

J. P. Rich · P. S. Doyle (✉)
Department of Chemical Engineering,
Massachusetts Institute of Technology,
Cambridge, MA, USA
e-mail: pdoyle@mit.edu

G. H. McKinley (✉)
Hatsopoulos Microfluids Laboratory,
Department of Mechanical Engineering,
Massachusetts Institute of Technology,
Cambridge, MA, USA
e-mail: gareth@mit.edu

Introduction

Magnetorheological (MR) fluids are field-responsive materials that exhibit fast, dramatic, and reversible changes in properties when subjected to a magnetic field. First introduced by Rabinow (1948), MR fluids are composed of microscopic iron-containing particles suspended in a matrix fluid. Upon application of a magnetic field, the particles acquire a dipole moment and align to form domain-spanning chains. This field-induced structuring of the suspension leads to significant changes in rheological properties, including order-of-magnitude growth in the steady-shear viscosity and the emergence of field-dependent yield stress and viscoelastic behavior (de Vicente et al. 2011a). The tunability of rheological properties with the applied magnetic field provides the basis for a wide variety of commercial applications of MR fluids, including automobile clutches (Rabinow 1948), active dampers (Spencer et al. 1997), seismic vibration control (Dyke et al. 1996), prosthetics (Carlson et al. 2001), precision polishing (Kordonski and Golini 1999), and drilling fluids (Zitha 2004). MR fluid research and technology

has been reviewed numerous times, with articles focusing on rheology and flow properties (de Vicente et al. 2011a), models and mechanisms of chain formation (Parthasarathy and Klingenberg 1996; Goncalves et al. 2006), MR fluid formulation (Park et al. 2010), and applications (Klingenberg 2001; Olabi and Grunwald 2007).

Matrix fluids in MR suspensions have traditionally been aqueous or oil-based Newtonian fluids of moderate viscosity. While this type of formulation maximizes the rheological differences between the activated material and the off-state, particle sedimentation is a major concern in Newtonian matrix fluids due to the (typically) large density difference between iron-containing particles and the surrounding fluid. To address this problem, modifications to both the suspended particles and the matrix fluid have been proposed. For example, according to the Stokes' drag law, sedimentation can be slowed by decreasing the particle size. Experiments have shown, however, that smaller particles generally lead to lower field-induced yield stresses (Lemaire et al. 1995). Additionally, when particle sizes approach nanometer length scales, Brownian effects limit the length and strength of the chain structures that form under an applied field (Fermigier and Gast 1992). Composite particles with lower iron content also exhibit slower sedimentation, but the accompanying decrease in magnetization again results in diminished field-induced rheological properties (Cho and Choi 2004). Reasonable success has been achieved through the use of stabilizing additives that provide a steric hindrance to particle aggregation. Additives such as ferromagnetic nanoparticles (Chin et al. 2001; Lopez-Lopez et al. 2005), fumed silica (Lim et al. 2004), organoclays (Lim et al. 2005), and magnetizable nanofibers (Ngatu et al. 2008) have been used for this purpose. Arguably the most robust methods for inhibiting sedimentation involve modifying the matrix fluid rheological properties. By employing viscoplastic matrix fluids (Rankin et al. 1999; Park et al. 2011) or thixotropic gel-forming agents such as silica nanoparticles (de Vicente et al. 2003; Lopez-Lopez et al. 2006), sedimentation can be prevented essentially indefinitely in quiescent dispersions as long as the yield stress of the matrix fluid exceeds the net stress acting on the particles due to gravity and buoyancy (Chhabra 1993).

For the set of experimental conditions considered by Rankin et al. (1999), results indicate that the matrix fluid yield stress has minimal effect on the field-induced dynamic yield stress. The field-induced *static* yield stress, however, is also an important property in many MR fluid applications and is a more direct measure of the "strength" of an MR fluid (Kordonski et al. 2001). The dynamic yield stress is typically measured by imposing a set of decreasing steady-state shear rates, $\dot{\gamma}$, and extrapolating the resulting shear stresses to $\dot{\gamma} = 0\ s^{-1}$. In contrast, the static yield stress is defined as the stress required to induce flow from rest (Nguyen and Boger 1992). For materials that exhibit thixotropy or require a finite time to reform microstructure after being sheared, these two yield stress measures are generally not equal (Møller et al. 2006, 2009; Bonn and Denn 2009). Additionally, in the case of MR fluids, it is reasonable to expect that the effects of a matrix fluid yield stress on field-induced structure and rheology will be more apparent in static yield stress measurements. The externally applied shear rate in dynamic measurements increases the probability that particles will encounter each other and aggregate despite the matrix fluid yield stress, whereas in static measurements magnetic particles must directly overcome the matrix fluid yield stress in order to form structure and provide an MR response. Because of these complications arising from differences in measuring techniques, and because of the practical utility of yield stress matrix fluids in inhibiting sedimentation, the need remains to develop a more thorough understanding of the effect of matrix fluid yield stresses on field-induced properties in MR fluids.

The yield stress matrix fluid in the current work is composed of an aqueous dispersion of the synthetic clay Laponite®. Often used as a rheological modifier in commercial soft materials, Laponite® clay consists of nanometric disks that undergo progressive structural arrest over time when dispersed in water at concentrations as low as about 1 wt% (Mourchid et al. 1995; Ruzicka et al. 2004, 2006; Jabbari-Farouji et al. 2008). This continual microstructural development, known as aging, results in complex and time-dependent rheology (Cocard et al. 2000; Joshi and Reddy 2008; Negi and Osuji 2010). Furthermore, the competition between aging and microstructural disruption due to shear (i.e. shear "rejuvenation") leads to thixotropic behavior (Abou et al. 2003). Previous work has addressed the bulk rheology and microrheology of aqueous Laponite® dispersions; for more thorough reviews of the current understanding of the phase behavior, structure, and rheology of aqueous Laponite® dispersions, see Ruzicka and Zaccarelli (2011) and Rich et al. (2011b). For the purposes of the current work, the significance of the aging behavior of Laponite® dispersions is that it results in continual growth of the static yield stress of the matrix fluid. Therefore, different matrix fluid yield stresses can be examined simply by allowing the MR composite system to age for different periods of time.

Using a custom-built magnetorheometry fixture (Ocalan 2011), the current work explores the field-induced static yield stress of MR suspensions in an aging, yield stress matrix fluid composed of an aqueous dispersion of Laponite®. The first section details the formulation of the composite MR fluid, including the aqueous Laponite® matrix fluid, and describes the custom magnetorheometry fixture and experimental protocol. Subsequently, we present results for the field-induced static yield stress as a function of magnetic field strength and age time. Field-induced dynamic and static yield stress measurements are compared at various particle concentrations, and observations are explained by considering the magnitude of appropriate dimensionless groups that characterize the balance between the matrix fluid yield stress and inter-particle magnetic stresses. The final section summarizes the key findings and identifies potential areas for future work.

Materials and methods

Magnetic particles and matrix fluid

The magnetic particles providing the MR response in the present study are CM grade carbonyl iron powder (CIP; BASF, Ludwigshafen, Germany). CM is a "soft grade" consisting of mechanically soft, approximately spherical particles with an iron content of about 99.5% by weight. Though the CM grade exhibits a wider size distribution than other CIP grades, it is also relatively economical. Figure 1a shows a scanning electron microscopy image of CIP, providing a sense for the polydispersity and irregularity of the particles. The scale bar corresponds to 5 μm. Particle size distributions of CIP, as measured with a Mastersizer 2000 particle size analyzer (Malvern Instruments, Worcestershire, UK), are shown in Fig. 1b. Both volume-weighted and number-weighted distributions are shown. The number-weighted distribution gives an average particle diameter of $\langle d \rangle \approx 3.7$ μm, with a standard deviation of about 2 μm. Additionally, from the volume-weighted distribution it is found that 50% of the powder volume consists of particles with diameter $d \leq d_{50} \approx 8.6$ μm, in quantitative agreement with data provided by the manufacturer.

Although the increased polydispersity and eccentricity of CIP particles can complicate analysis, the use of CIP in MR fluids provides functional advantages over polymer–magnetite composite superparamagnetic particles because of its stronger magnetic properties, which result from the high iron content. Figure 1c shows magnetization data for CIP, obtained using a vibrating sample magnetometer with a sample of approximately 0.02 g of CIP powder. The particles exhibit linear magnetization up to an applied magnetic field of about $B \approx 0.1$ T. Beyond about $B \approx 0.6$ T, the particles exhibit a constant saturation magnetization of about $M_{sat} \approx 190$ emu $g^{-1} = 190$ A m^2 kg^{-1}, which is about ten times greater than that of similar-sized polymer–magnetite superparamagnetic particles (based on data from manufacturer, Invitrogen). Though a small remnant

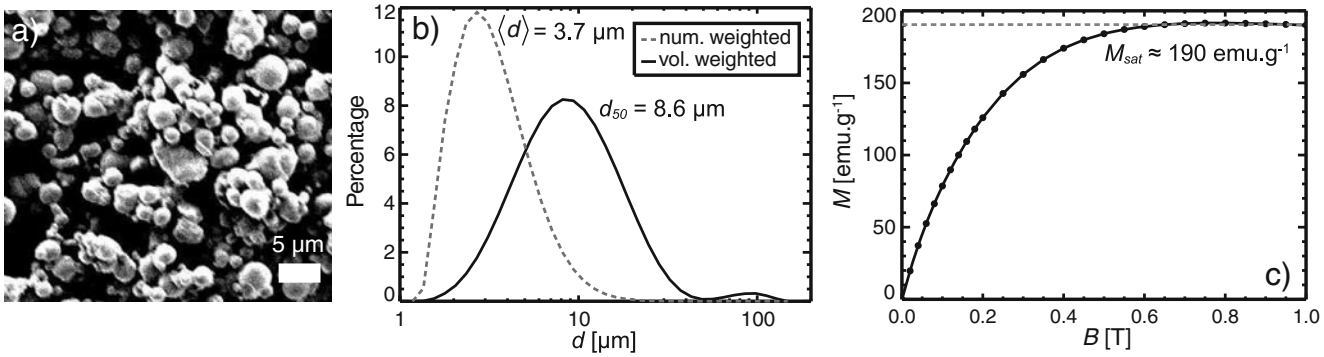

Fig. 1 The magnetic component of the magnetorheological fluid in the present study is CM grade Carbonyl Iron Powder (CIP; BASF, Ludwigshafen, Germany). **a** Scanning electron microscopy (SEM) image of CIP. The powder consists of approximately spherical particles exhibiting some polydispersity and irregularity. **b** Volume-weighted and number-weighted size distributions of CIP particles in the present study. Treating CIP particles as spherical, an average particle diameter of about 3.7 μm is extracted from the number-weighted distribution. Additionally, the volume-weighted distribution indicates that 50% of the powder volume consists of particles with effective diameter $d \leq d_{50} = 8.6$ μm, in agreement with data provided by the manufacturer. **c** CIP magnetization curve. Solid lines connect data points and serve to guide the eye. According to the manufacturer's specifications, the particles are ≥99.5% Fe, leading to large values of the magnetization M at moderate applied fields. The particles exhibit linear magnetization for small applied fields ($B \leq 0.1$ T) and reach a saturation magnetization of about $M_{sat} \approx 190$ emu g^{-1}, denoted by the dashed gray line, above about $B \approx 0.6$ T

magnetization (∼1 emu/g) has previously been reported for similar types of magnetic particles (Phulé et al. 1999), our measurements indicate negligible magnetic hysteresis for $B \geq 0.05$ T.

In the present study, CIP is suspended in an aging, yield stress matrix fluid, and the MR response of the composite is explored. The matrix fluid consists of a 3.0 wt% aqueous dispersion of the synthetic colloidal clay Laponite® (RD grade, Southern Clay Products, Gonzales, TX). To prepare a sample, dry Laponite® powder is added to an aqueous buffer of pH ≈ 10 consisting of 1.8 mM NaOH and 4.1 mM $NaHCO_3$. The purpose of the buffer is to avoid the slow dissolution of Laponite® platelets, which has been observed at lower pH (Thompson and Butterworth 1992), and to fix the solvent ionic strength at $I = 5.9$ mM. During mixing, the dispersion is kept under N_2 gas in order to prevent the uptake of CO_2, which can lower the solution pH and contribute to the dissociation of platelets (Mourchid et al. 1995; Mourchid and Levitz 1998; Martin et al. 2002). After mixing vigorously for at least 1.5 h, the clay dispersion is passed through a 0.8-μm filter, breaking apart most of the remaining aggregates with a strong shear field (Bonn et al. 1999). Petit et al. (2009) demonstrated that about 7% of the initial Laponite® concentration is lost when dispersions of about 3 wt% Laponite® are passed through 0.45 μm filters. However, since the present study uses filters with larger pores (0.8 μm), it is assumed that filtration does not appreciably change the nominal concentration of Laponite®. Immediately after filtering, CIP is added to the desired concentration; and after vortex mixing for about 30 s, the CIP is dispersed approximately homogeneously. The composite suspension is then deposited onto the sample plate of the custom MR cell described below.

Bulk magnetorheology

The bulk rheology of CIP suspended in aqueous Laponite® dispersions is studied under applied magnetic fields using the custom-built magnetorheology fixture designed by Ocalan (2011) that is shown in Fig. 2. The magnetic field is generated by passing electrical current (up to 5 A) through a coil of copper magnet wire, which is wrapped around a cylindrical core of 1018 carbon steel. The fluid sample is placed between a non-magnetic aluminum sample plate, which is fixed directly above the cylindrical core, and a 20 mm diameter non-magnetic titanium plate geometry that is attached to the spindle rod of the rheometer. To minimize wall-slip, the aluminum sample plate is sand-blasted to an RMS roughness of about 3.8 μm, and adhesive-backed 600 grit sandpaper disks (McMaster-Carr, Elmhurst, IL, RMS roughness ≈ 6.0 μm) are attached to the 20 mm top plate. An elastomeric ring

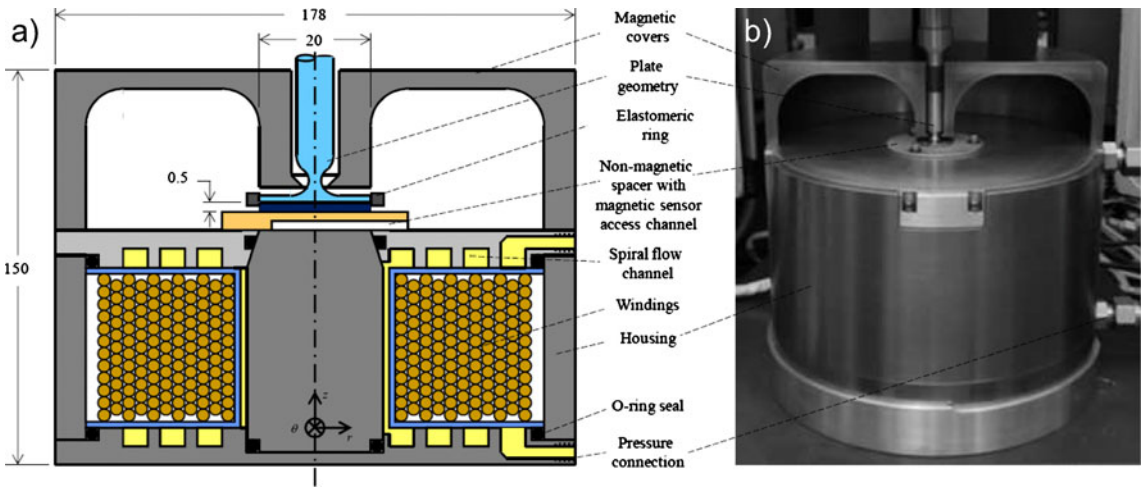

Fig. 2 The custom-built fixture used for magnetorheology experiments shown **a** as a cross-sectional schematic and **b** mounted on a stress-controlled rheometer [images reproduced with permission from Ocalan (2011)]. Dimensions are given in millimeters. The magnetorheometry fixture consists of copper magnet wire wrapped around a cylindrical core of 1018 carbon steel. The fluid sample fills the space between a non-magnetic aluminum sample plate and a 20 mm diameter non-magnetic plate of titanium alloy that is attached to the spindle rod of the rheometer. Silicone oil flows through channels surrounding the coil, providing temperature control. Two cover plates of 1018 carbon steel complete the magnetic circuit, helping to direct the field uniformly through the sample. A thin slot in the bottom of the sample plate allows access for a Gauss probe to measure the magnitude of the applied magnetic field. When a current of about 3.5 A passes through the coil, the setup can apply magnetic fields up to $B \approx 1$ T with high spatial uniformity

on the outer edge of the top plate helps to prevent the sample from escaping from the gap and climbing the spindle rod in response to strong magnetic fields. A thin slot in the bottom of the sample plate provides access for a Gauss probe to measure the magnetic field directly beneath the sample. The entire fixture is housed in a casing of 1018 carbon steel, including a top cover that serves to complete the magnetic circuit and direct the magnetic field through the sample, and then mounted on a stress-controlled rheometer (ARG-2, TA Instruments, New Castle, DE). The casing and cover design prevent the applied magnetic fields from interfering with the magnetic bearing of the rheometer. Temperature control is achieved by flowing silicone oil through channels machined within the casing. Using the fixture, highly uniform magnetic fields up to $B \approx 1$ T can be applied to the sample. For more detailed information about the design of the fixture, its capabilities, and analysis of the applied fields, see Ocalan (2011).

After preparing the sample as described above, the fluid is introduced between the rheometer plates and the gap height is set to 0.5 mm. Because of the thixotropic nature of the Laponite® matrix fluid, steps are taken to ensure consistent initial conditions and promote reproducibility of results. Initially, the sample is pre-sheared at a rate of $\dot{\gamma} = 600\ \mathrm{s}^{-1}$ for 10 s, effectively erasing the shear history and resetting the age time, t_w, to zero (Fielding et al. 2000; Bonn et al. 2002). Though it has been shown that even a strong shear cannot completely 'rejuvenate' the aging process in aqueous Laponite® dispersions (Shahin and Joshi 2010), this small amount of irreversibility is found to have a negligible effect on the rheological response of the composite to magnetic fields. Subsequent to the pre-shear at $\dot{\gamma} = 600\ \mathrm{s}^{-1}$, the magnetic component of the suspension is structured by applying a relatively high magnetic field of 0.8 T for 30 s, after which the field is switched off and the material is pre-sheared again at $\dot{\gamma} = 250\ \mathrm{s}^{-1}$ for 20 s. Pre-shearing for longer periods of time had negligible effect on results. This protocol provides consistent magnetic and shear histories and imposes reproducible initial conditions for magnetorheology experiments (Deshmukh 2006). The suspension is allowed to age at a constant temperature $T = 22.5°\mathrm{C}$, and the desired magnetic field is applied starting 30 s before performing rheometric tests to probe the yielding behavior. Initiating the magnetic field at times from about 15 s to 1 min prior to the start of rheometric tests did not significantly affect results. The primary focus of the present work is the static yield stress, which is measured using continuous ramp tests; starting from a value below the static yield stress, the applied shear stress is increased continuously until the dispersion has yielded, allowing the extraction of the flow curve during yielding. The stress is ramped linearly over a test time of $\Delta t_{test} = 2$ min ($\Delta t_{test} = 1$ min for 10 min age samples), which is small compared to the age of the dispersion t_w. Though attempts are generally made to minimize the rate of stress increase, as long as the initial stress is sufficiently below the static yield stress and $\Delta t_{test} \ll t_w$, the exact rate of stress increase has minimal effect on the results. We note that because the stress is ramped continuously, the measured flow curves do not necessarily correspond precisely to steady-state measurements. However, steady-state measurements would generally be complicated by the aging behavior of the Laponite® matrix fluid (Fielding et al. 2000), so that in this case the continuous ramp tests provide a consistent and meaningful measure of the static yield stress at a particular age time when $\Delta t_{test}/t_w \ll 1$. To measure the dynamic yield stress, steady-state flow tests are performed in which the shear rate is decreased logarithmically in discrete steps from $\dot{\gamma} = 100\ \mathrm{s}^{-1}$ to $\dot{\gamma} = 0.05\ \mathrm{s}^{-1}$. Starting from higher shear rates has negligible effect on the extracted values of the dynamic yield stress. Because the aging behavior of the matrix fluid can lead to continually evolving properties, a relatively lenient criteria for reaching steady-state is used (two consecutive 3-second measurements giving results within 5% of each other), so that the time required for a test remains small compared to the age time (about 1 min). The dynamic yield stress is obtained by extrapolating the measured stress values to $\dot{\gamma} = 0\ \mathrm{s}^{-1}$ (Nguyen and Boger 1992).

Results and discussion

Effects of magnetic field and aging

In Newtonian matrix fluids, chain models for electro- and magnetorheology predict that the yield stress will increase quadratically with the magnetic field B for low field strengths when the magnetic particles are in the linear magnetization regime (Klingenberg and Zukoski 1990). As the magnetic field increases and the particles exhibit nonlinear magnetization, the yield stress is predicted to scale as $B^{3/2}$ and eventually become independent of B as the particle magnetization saturates (Ginder et al. 1996). These scalings have been confirmed experimentally for spherical particles (Chin et al. 2001; de Vicente et al. 2010), though some studies have reported a somewhat weaker dependence on B (Bossis et al. 2002; Bossis and Lemaire 1991). For MR suspensions stabilized by single-walled carbon nanotubes, Fang et al. (2009) reported a transition in

the scaling of the yield stress from B^2 to $B^{3/2}$ with increasing magnetic field. Similar observations have been made in some ER fluid systems (Zhang et al. 2010). In matrix fluids composed of viscoplastic grease, Rankin et al. (1999) reported that the field-induced dynamic yield stress scales with B^x, where x decreases from about 1.5 to 0 as the magnetic field increases and the magnetization of the particles saturates. The value of $x = 1.5$ in grease-based matrix fluids for magnetic fields below the saturation regime (about 0.05 T to 0.35 T) has also been reported by other authors (Park et al. 2001, 2011).

Flow curves from continuous stress ramp tests under magnetic fields are shown in Fig. 3. The sample consists of 10 v% CIP (47 wt% CIP) in a 3.0 wt% aqueous Laponite® dispersion at an age time of $t_w = 10$ min. The constant age time ensures consistent matrix fluid properties for each measurement. For each value of the magnetic field, very small shear rates are observed until a critical shear stress is exceeded, after which the shear rate abruptly increases by several orders of magnitude. This behavior is a definitive characteristic of field-activated yield stress fluids, and indicates a breaking of the field-induced microstructure at the critical applied stress, which corresponds to the static yield stress, τ_{ys}. Larger values of this critical stress are observed as the magnetic field is increased; at $B = 1.0$ T, the material can support stresses about four to five times higher than at $B = 0.2$ T without yielding. Beyond about $B = 0.6$ T,

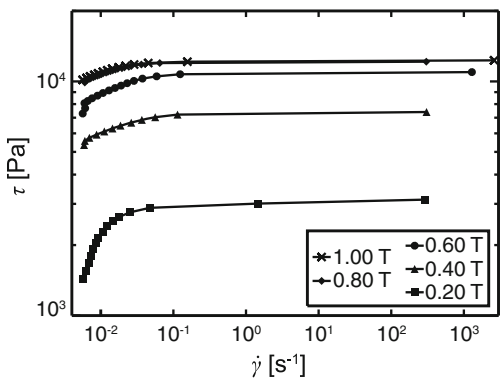

Fig. 3 Typical flow curves from continuous stress ramp tests at various applied magnetic fields. Lines connect data points to guide the eye. The qualitative trends in the data above, which correspond to a 10 v% CIP suspension in a 3.0 wt% aqueous Laponite® dispersion at an age time of 10 min, are representative of all CIP concentrations and age times. At a given magnetic field, the shear rate is negligibly small up to a critical shear stress that corresponds to the field-induced static yield stress, τ_{ys}. Further increasing the applied stress results in the shear rate increasing by several orders of magnitude. Note that since the stress is ramped continuously, the data above do not necessarily correspond directly to steady-state measurements

the response of the material to applied stress changes minimally with increasing magnetic field, which is a result of the magnetic saturation of the particles at these higher field strengths. While the measured shear rates in these experiments may not necessarily correspond precisely to steady-state measurements, as described above, by maintaining consistent experimental conditions it is possible to extract meaningful and repeatable values of the field-induced static yield stress, τ_{ys}, which is determined as the critical stress above which an abrupt increase in the shear rate is observed (Nguyen and Boger 1992).

The field-induced static yield stress for 10 v% CIP is shown as a function of the magnetic field strength, B, in Fig. 4a. The age time for the 3.0 wt% aqueous Laponite® matrix fluid is again kept constant at $t_w = 10$ min. Error bars represent the standard deviation between measurements on three different samples, providing an indication of the reproducibility of the measurements. For applied fields of 0.1 T to 0.5 T, τ_{ys} grows approximately linearly with B. As the magnetic field is increased further, a plateau is observed so that for fields above about $B \approx 0.6$ T, τ_{ys} is approximately independent of the magnetic field. This regime is again indicative of the magnetic saturation of CIP particles. Before the onset of magnetic saturation, the magnetic field has a strong effect on the rheology; τ_{ys} increases by about an order of magnitude from $B = 0.1$ T to $B = 1.0$ T. These trends are qualitatively similar to those reported in Newtonian matrix fluids (Ginder et al. 1996). Though the regime of quadratic dependence on B predicted for Newtonian matrix fluids has not been observed, this is likely because the particles already begin to exhibit nonlinear magnetization effects at $B = 0.1$ T (see Fig. 1c).

A unique aspect of the aqueous Laponite® matrix fluid used in the present study is its aging behavior. Left quiescent, the rheological properties of the Laponite® dispersion evolve with time as individual clay particles coordinate and an arrested microstructure develops in the material (Ruzicka and Zaccarelli 2011). Aging results in growth of both the yield stress and the matrix viscoelasticity (Rich et al. 2011a, b), and generally leads to a more solid-like material. Figure 4b shows the effect of this aging in the matrix fluid on the magnetorheology of the 10 v% CIP suspension. Squares represent the static yield stress of the 3.0 wt% Laponite® matrix fluid with no added CIP, which grows steadily with age time as expected. Without a magnetic field, adding CIP to the matrix fluid raises the static yield stress by at most 60% (at 30 v% CIP), which is small compared to the field-induced gain in the yield stress. For an applied field of $B = 0.1$ T, a small increase in the field-induced

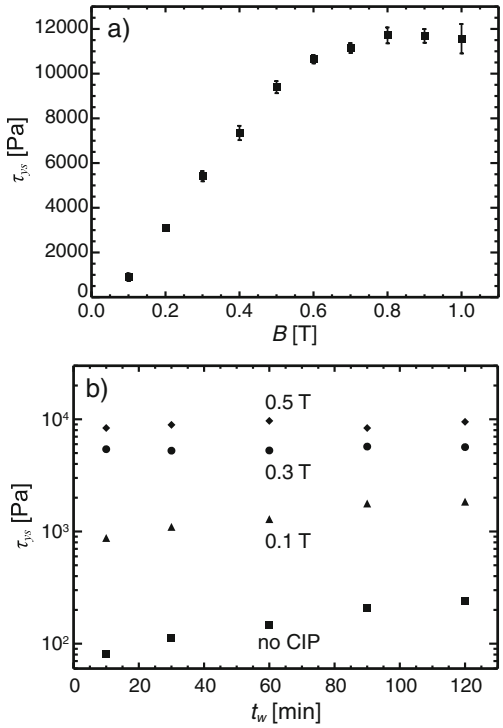

Fig. 4 Field-induced static yield stress, τ_{ys}, of a 10 v% CIP suspension in a 3.0 wt% aqueous Laponite® dispersion. **a** Field-induced static yield stress as a function of the applied magnetic field, B, at an age time of $t_w = 10$ min (matrix fluid static yield stress, $\tau_{ys,0} \approx 85$ Pa). *Error bars* represent the standard deviation of measurements on three different samples. At low field strengths, τ_{ys} increases with the applied magnetic field, B. Saturation of the yield stress is observed for B greater than about 0.6 T, due primarily to the saturation of the particle magnetization (see Fig. 1c). τ_{ys} grows by more than an order of magnitude from $B = 0.1$ T to $B = 1.0$ T. **b** Static yield stress as a function of age time, t_w, for 3.0 wt% aqueous Laponite® dispersions with no added CIP and with 10 v% CIP at $B = 0.1$, 0.3, and 0.5 T. While the matrix fluid yield stress increases with age time, the yield stress of the composite is essentially independent of age time (i.e., independent of the matrix fluid yield stress) for all but the lowest magnetic field. The addition of CIP and magnetic fields as low as $B = 0.1$ T results in an order of magnitude increase in the static yield stress over that of the matrix fluid alone

static yield stress is observed between $t_w = 10$ min and $t_w = 120$ min. For larger magnetic fields, however, τ_{ys} becomes essentially independent of age time, indicating an insensitivity to matrix fluid properties. Two orders of magnitude separate the values of τ_{ys} for the pure matrix fluid and data for a 10 v% dispersion at $B = 0.5$ T, which again highlights the strong effect of the magnetic field on the rheology.

The independence of τ_{ys} on the matrix fluid rheological properties for moderate to high magnetic field strengths can be understood by considering the relative magnitude of the different stresses acting on the CIP particles. Specifically, and in analogy with the approach of Rankin et al. (1999), the matrix fluid yield stress can be compared to the inter-particle dipolar stress resulting from the applied magnetic field. If mutual magnetic induction is neglected so that all the particles are assumed to have the same constant dipole moment, the interaction energy U_{ij} between two spherical dipoles with centers separated by a distance r_{ij} and subject to a uniform external magnetic field is

$$U_{ij} = \frac{m^2 \mu_0}{4\pi} \left(\frac{1 - 3\cos^2 \theta}{r_{ij}^3} \right) \tag{1}$$

where m is the dipole moment, μ_0 is the magnetic permeability of the medium (assumed to be equal to the permeability of free space), and θ is the angle that the line connecting the particle centers makes with the direction of the applied magnetic field. The attraction force between the particles is maximum when their centers are aligned with the field ($\theta = 0$). In this case, the magnitude of the force is

$$F_{ij}\big|_{\theta=0} = \left| -\frac{dU_{ij}(\theta = 0)}{dr_{ij}} \right| = \frac{3m^2 \mu_0}{2\pi r_{ij}^4} \tag{2}$$

This expression can be used to find a characteristic force by setting r_{ij} to the particle diameter, d, which is the minimum distance between particle centers. A characteristic magnetic force between particles is therefore

$$F_{char} = \frac{\pi}{24} d^2 \mu_0 (\rho M)^2 \tag{3}$$

Here the dipole moment has been expressed as $m = (\pi/6)\, d^3 \rho M$ where ρ is the particle density and M is the magnetization per unit mass. A characteristic magnetic stress can be found by dividing Eq. 3 by the surface area of a spherical particle πd^2

$$\tau_{char} = \frac{\mu_0 (\rho M)^2}{24} \tag{4}$$

Comparing the characteristic values obtained from Eq. 4 to the static yield stress of the matrix fluid, $\tau_{ys,0}$, which must be overcome for the particles to move and form a chain-like structure in response to the imposed field, provides insight into the effect of the matrix fluid on the MR response. This balance of stresses is characterized by the following dimensionless group

$$\mathrm{Y}_{\mathrm{M}}^{*} = \frac{\mu_0 (\rho M)^2}{24 \tau_{ys,0}} \tag{5}$$

This parameter is similar to the so-called "magnetic yield parameter" introduced by previous authors (Rankin et al. 1999). Generally, if $\mathrm{Y}_{\mathrm{M}}^{*} > 1$ chain-like structures will form under the action of an external magnetic field and a bulk MR response will be observed, whereas if $\mathrm{Y}_{\mathrm{M}}^{*} \ll 1$, the yield stress of the matrix

fluid prevents structure formation. For the magnetic CIP particles used in the present experiments, the density of iron is $\rho \approx 7.8$ g cm^{-3}, and the magnetization data in Fig. 1c shows that for $B \geq 0.2$ T, $M \sim 100$ emu g^{-1} = 100 A m^2 kg^{-1}. Figure 4b shows that the static yield stress of the matrix fluid is on the order of 100 Pa. Using these numerical values in Eq. 5 gives $Y_M^* \approx 320 \gg 1$. Therefore, the characteristic magnetic stress between particles is much greater than the matrix fluid yield stress. As a result, it is reasonable to expect that moderate changes in the matrix fluid yield stress during aging will have minimal effect on the magnetorheological response. For the case of $B = 0.1$ T, it is helpful to return to Eq. 2 and recognize that the average distance between particle centers is dependent on the volume fraction of CIP, ϕ_{CIP}. Treating the CIP suspension as a homogeneous dispersion of monodisperse spheres, this volume fraction dependence can be accounted for in an approximate way by replacing r_{ij} with $d\phi_{CIP}^{-1/3}$ rather than simply d. Carrying this change through Eqs. 3–5 results in a modification to Y_M^*

$$Y_{M,\phi}^* = \frac{\mu_0 (\rho M)^2}{24\tau_{ys,0}} \phi_{CIP}^{4/3} \tag{6}$$

Applying data from Figs. 1c and 4b for a 10 v% CIP dispersion at $B = 0.1$ T and a matrix fluid age time of $t_w = 120$ min results in a value of $Y_{M,\phi}^* \approx 4$. The fact that $Y_{M,\phi}^*$ is close to 1 in this case implies that the characteristic magnetic stress on particles exceeds the matrix fluid yield stress by only a small amount. The magnetorheological response of the composite is therefore expected to reflect a combination of the structures formed by magnetic particles as well as the matrix fluid rheology. This is consistent with the observation that the matrix fluid and the 10 v% CIP composite at $B = 0.1$ T exhibit similar rates of growth in the static yield stress during aging. For reference, in the case of a 10 v% CIP dispersion and a matrix fluid age time of $t_w = 120$ min, $Y_{M,\phi}^* \approx 15$ at $B = 0.3$ T, so that matrix fluid effects are again expected to be minimal for this higher magnetic field strength.

An important complication in microstructured fluids is that rheological properties measured at the bulk scale often do not entirely reflect behavior and properties at the microscopic scale (Waigh 2005; Liu et al. 2006). In the present experiment, suspended CIP particles have an average diameter of about 3.7 μm (see Fig. 1b), so the yield stress of the matrix fluid measured via bulk rheology may not be representative of the matrix fluid yield stress at the length scale of the magnetic microparticles. This effect could result from pores or other microstructures in the matrix fluid that have similar length scales as the CIP particles. This question was addressed in a previous communication (Rich et al. 2011a) in which bulk yield stress values were compared to nonlinear microrheology magnetic tweezer measurements in aqueous Laponite® dispersions. The probes for microrheology experiments were superparamagnetic spheres of diameter 4.5 μm, which is similar to the average size of CIP particles in the current work. For Laponite® concentrations greater than or equal to about 2.0 wt%, bulk and micro-scale yield stress measurements were found to agree quantitatively so long as differences in the flow kinematics for the two experiments are correctly taken into account. This kinematic correction consists of an order one factor that approximately captures the shear contribution to the applied stress in the micro-scale experiment involving spherical probe particles. Since the Laponite® concentration in the present work is 3.0 wt%, and since the CIP particles are irregular in shape (see Fig. 1a), we neglect this correction factor and consider the matrix fluid yield stress measured via bulk experiments also to be representative of that on the length scale of the CIP particles. Further, since the value of the matrix fluid yield stress is used primarily to gain physical insight by evaluating the dimensionless yield parameters defined in Eqs. 5 and 6, an order one correction factor will have negligible effect on conclusions.

The observation that the field-induced static yield stress is largely independent of the matrix fluid static yield stress is consistent with the results of Rankin et al. (1999), who showed similar behavior for the field-induced dynamic yield stress of CIP suspensions in viscoplastic greases. Because of the nature of dynamic yield stress measurements, in which an initial applied shear rate increases the probability that magnetic particles will encounter each other and form chains, and because the measured field-induced dynamic yield stresses exceeded the matrix fluid yield stresses by 2 to 3 orders of magnitude, it is to be expected that the MR dynamic yield stresses measured in the work of Rankin et al. (1999) would be relatively independent of matrix fluid properties. For field-induced static yield stress measurements, however, the matrix fluid properties can play a more significant role because the magnetic particles must overcome the matrix fluid yield stress in order to form the chain-like structure and provide an MR response. It is therefore unclear a priori whether field-induced static yield stress measurements in yield stress matrix fluids would exhibit a similar insensitivity to matrix fluid properties as in the case of dynamic measurements. From the perspective of formulators of MR fluids, independence of the field-induced yield stress on matrix fluid rheology is likely to be an attractive

and advantageous property. As long as the matrix fluid yield stress is sufficient to prevent magnetic particle sedimentation, the exact rheological properties of the matrix fluid have little bearing on the field-responsive rheology. Therefore, the matrix fluid rheology can be optimized to meet various off-state needs or designed for other functionalities with little concern for how the activated material will behave. Care must be taken to account for matrix fluid rheological properties, however, at low field strengths and large matrix fluid yield stresses, as has been discussed. The following section, which examines the role of magnetic particle concentration, shows that effects of the matrix fluid yield stress must also be taken into consideration at low volume fractions of magnetic particles, as implied by Eq. 6.

Effect of magnetic particle concentration

Increasing the concentration of magnetic particles generally enhances the rheological response of MR fluids to an applied magnetic field (Goncalves et al. 2006). For this reason, volume fractions in commercial applications are often as high as 40 to 50 v% (Jolly et al. 1999), despite the fact that increased concentrations of magnetic particles also result in an elevated off-state viscosity. Established models predict that the field-induced yield stress and viscoelastic storage modulus (Ginder et al. 1996), as well as the viscosity (Martin and Anderson 1996), will exhibit a linear dependence on the volume fraction of magnetic particles (de Vicente et al. 2011a). While experimental results for the field-induced dynamic yield stress have corroborated this linear relationship up to surprisingly high concentrations in both Newtonian and non-Newtonian matrix fluids, a super-linear increase with volume fraction has been observed above about $\phi_{\mathrm{CIP}} = 0.2$ (Felt et al. 1996; Rankin et al. 1999; Chin et al. 2001; Volkova et al. 2001). This behavior is thought to result from the formation of thick columnar structures, as opposed to the single particle-width chains that dominate at low concentrations.

In Fig. 5 we show the dependence of the field-induced yield stress on the magnetic field strength, B, for suspensions with different volume fractions of CIP. The matrix fluid is a 3.0 wt% aqueous Laponite® dispersion at a constant age time of $t_w = 10$ min ($\tau_{ys,0} \approx 85$ Pa). Filled symbols and solid lines represent the static yield stress, τ_{ys}, while open symbols and dashed lines represent the dynamic yield stress, τ_{yd}, which has typically been reported by previous authors for MR composites in yielding matrix fluids such as greases (Rankin et al. 1999; Park et al. 2011). For all CIP concentrations, both yield stress measures grow with

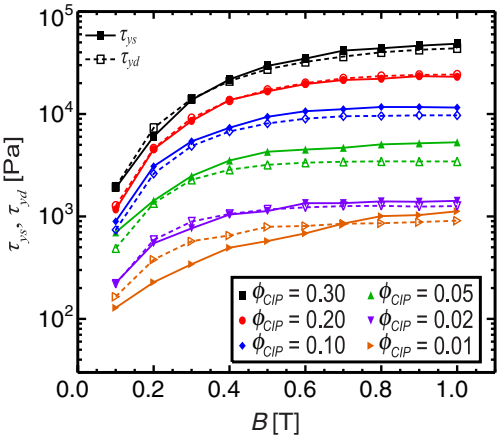

Fig. 5 Field-induced yield stress as a function of magnetic field for various CIP volume fractions, ϕ_{CIP}, in a 3.0 wt% aqueous Laponite® dispersion at an age time of $t_w = 10$ min. Both the static yield stress, τ_{ys} (*filled symbols and solid lines*), and the dynamic yield stress, τ_{yd} (*open symbols and dashed lines*), are shown. For all CIP concentrations considered in the present study, both measures of the yield stress follow a similar trend with the applied magnetic field, growing with B and exhibiting a plateau above about 0.6 T. Good agreement is observed between the field-induced static and dynamic yield stresses for all but the lowest CIP concentration at low magnetic fields

the magnetic field up to about $B = 0.6$ T, beyond which a plateau is observed. This trend is generally consistent with previous measurements of τ_{yd} in yield stress matrix fluids (Rankin et al. 1999), though the plateau in Fig. 5 begins at slightly higher field strengths (most likely due to a different size and grade of CIP). For the largest volume fraction examined in the present work, field-induced static and dynamic yield stresses up to about 50 kPa are observed. Because the matrix fluid yield stress is significantly larger than the gravitational stress acting on particles and continually grows as the dispersion ages, sedimentation is prevented essentially indefinitely for all CIP concentrations examined. Based on these results, it is reasonable to anticipate that gravitationally stable dispersions with higher field-induced yield stresses could be achieved by further increasing the CIP concentration to 40 or 50 v%.

With the exception of results for the lowest CIP concentration at low applied fields, the two measures τ_{ys} and τ_{yd} are in good agreement, indicating that field-induced thixotropy is negligible. This is despite the thixotropic nature of the aqueous Laponite® matrix fluid; at $t_w = 10$ min, $\tau_{ys,0} \approx 85$ Pa while the matrix fluid dynamic yield stress is measured to be $\tau_{yd,0} \approx 20$ Pa. The deviation between τ_{ys} and τ_{yd} at $\phi_{CIP} = 0.01$ and low applied magnetic fields is most likely due to the inability of some dispersed magnetic particles to overcome the matrix fluid yield stress and

form gap-spanning chains during the static yield stress measurement (Rich et al. 2012). In this dilute dispersion, for which the average distance between particles is relatively large, inter-particle attractive forces at low external fields may be insufficient to overcome the matrix fluid yield stress. Quantitatively, for $\tau_{ys,0} = 85$ Pa, $\phi_{CIP} = 0.01$, and $B = 0.2$ T ($M \approx 125$ emu g^{-1}, see Fig. 1c), inserting parameters into Eq. 6 gives a volume-fraction corrected yield parameter of $Y^*_{M,\phi} = 1.3$. Values close to unity indicate that the matrix fluid yield stress approximately balances attractive forces between particles resulting from dipolar interactions, hindering chain formation. In the dynamic yield stress measurement, however, bulk shear and rejuvenation of the matrix fluid disrupt and lower the matrix yield stress, enabling viscous flow and increasing the likelihood that particles will aggregate and form chains, as discussed above. Therefore, deviations between τ_{yd} and τ_{ys} are reasonable in this dilute regime at low magnetic field strengths. In particular, the observation that $\tau_{yd} > \tau_{ys}$, in contrast to the case of the pure matrix fluid, is consistent with the mechanism described above.

Figure 5 shows that the field-induced static and dynamic yield stresses increase substantially with CIP concentration. This behavior is specifically highlighted in Fig. 6a, where the yield stress results are plotted as a function of ϕ_{CIP} for constant values of the applied magnetic field. For clarity, only static yield stress measurements for three representative field strengths are shown ($B = 0.1$, 0.2, and 0.5 T), though the dynamic yield stress data is generally quantitatively similar, as previously discussed. At a given field strength, the yield stress increases by more than an order of magnitude from $\phi_{CIP} = 0.01$ to $\phi_{CIP} = 0.30$. A nearly linear dependence on CIP volume fraction is observed, though a more general power-law relationship is most appropriate

$$\tau_{ys} = K\phi^a_{CIP} \tag{7}$$

The coefficient κ and the power-law exponent α depend on the field strength. Least-squares fits to Eq. 7 are shown by black lines. The ability of the power-law form to characterize the data in Fig. 6a is representative of the goodness of fit for other field strengths, and the power-law fits provide a minimum coefficient of determination of $R^2 = 0.96$. The variation of the fitted parameters in Eq. 7 with the applied magnetic field is shown in Fig. 6b for both the static (filled symbols) and dynamic (open symbols) yield stresses. Squares specify the power-law exponent α on the left axis, and circles give the coefficient κ on the right axis. κ values reflect the behavior of the field-induced yield stress,

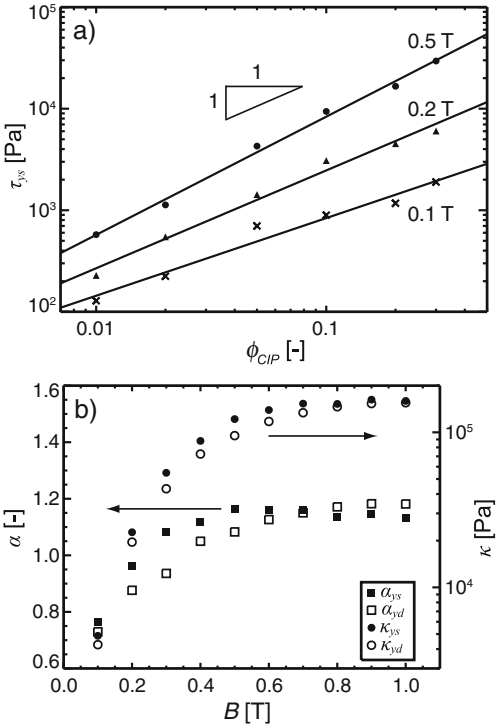

Fig. 6 **a** Variation of the field-induced yield stress with CIP volume fraction in a 3.0 wt% aqueous Laponite® dispersion at an age time of $t_w = 10$ min. For clarity, only static yield stress data at three representative field strengths are shown here, but both τ_{ys} and τ_{yd} exhibit a similar power-law dependence on ϕ_{CIP} for all field strengths. The magnitude of τ_{ys} (as well as τ_{yd}) increases by almost two orders of magnitude from $\phi_{CIP} = 0.01$ to $\phi_{CIP} = 0.30$. In **b**, the power-law exponents, α, and coefficients, κ, resulting from least-squares fitting to Eq. 7 (for which the minimum coefficient of determination is $R^2 = 0.96$), are shown for the field-induced static (*filled symbols*) and dynamic (*open symbols*) yield stresses. Squares represent the exponent α, given on the left axis, while circles represent the front factor κ, given on the right axis. The coefficient κ grows with the magnetic field in a manner that reflects the field dependence of the yield stress, as shown in Fig. 5. Both sets of power-law exponents increase from $\alpha \approx 0.75$ at $B = 0.1$ T (sub-linear dependence on ϕ_{CIP}) to $\alpha \approx 1.15 \pm 0.06$ for B greater than about 0.5 T (super-linear dependence on ϕ_{CIP})

increasing by almost two orders of magnitude from $B = 0.1$ T to $B = 1$ T and exhibiting saturation above about $B = 0.6$ T. Additionally, κ values fitted from static and dynamic yield stress data are in good agreement. While all α values are close to unity, signifying a nearly linear dependence of the yield stress on CIP volume fraction as mentioned above, there is a clear trend in which α increases from $\alpha \approx 0.75$ at $B = 0.1$ T to $\alpha \approx 1.15$ above about $B = 0.5$ T. This indicates that the yield stress increases sub-linearly with ϕ_{CIP} for low field strengths, and super-linearly above about $B = 0.5$ T. The power-law exponents for τ_{ys} and τ_{yd} are in good agreement, deviating by less than 15%. The sub-linear

volume fraction dependence of the field-induced yield stress observed here at low field strengths is in contrast to model predictions (Ginder et al. 1996) and previous experimental results (Felt et al. 1996) for Newtonian matrix fluids, which show a linear dependence on magnetic particle concentration for low field strengths and dilute suspensions. Additionally, previous studies of MR composites in a viscoplastic grease have reported a linear dependence on the volume fraction for $B \approx 0.05$–0.2 T and $\phi_{CIP} = 0.02$–0.25 (Rankin et al. 1999). These discrepancies are again most likely related to the balance between inter-particle magnetic stresses and the matrix fluid yield stress (Rich et al. 2012). For example, for $B = 0.1$ T, $Y^*_{M,\phi}$ grows from 0.5 to 50 as ϕ_{CIP} is increased from 0.01 to 0.30, implying that measurements will reflect a relative contribution of the matrix fluid yield stress that diminishes as the CIP concentration is increased. The fact that τ_{ys} remains close to the matrix fluid yield stress ($\tau_{ys,0} = 85$ Pa) for $B = 0.1$ T at low CIP concentrations is further evidence for the effect of the matrix fluid. As the CIP concentration increases and $Y^*_{M,\phi}$ becomes much greater than unity, the magnetic response is expected to dominate the matrix fluid yield stress. Fitting Eq. 7 to data spanning this range of $Y^*_{M,\phi}$ values results in a power-law exponent that averages the behavior in these two regimes and indicates a sub-linear dependence of the field-induced yield stress on CIP volume fraction. We note that the volume-fraction corrected yield parameter has values $Y^*_{M,\phi} \geq 5$ under the conditions examined in the work of Rankin et al. (1999), assuming similar magnetization properties as reported in Fig. 1c.

Figure 5 shows that the field-induced yield stresses of MR composites with different CIP concentrations exhibit similar trends with magnetic field strength, despite differences in the magnitude of the yield stress. This observation motivates the question of whether the data can be shifted to generate one master curve relating the field-induced yield stress to the magnetic field for different values of ϕ_{CIP}. Such a master curve is shown in Fig. 7a, where the field-induced static yield stress data from Fig. 5 is shown as a reduced yield stress, $b\tau_{ys}$, plotted as a function of a reduced magnetic field strength, $a_B B$. By employing the horizontal and vertical shift factors a_B and b, respectively, yield stress data for different CIP concentrations has been collapsed onto a single master curve that increases with the magnitude of the reduced magnetic field. The data has been shifted to a reference concentration of $\phi_{CIP} = 0.10$. The fact that such a master curve can be generated suggests the systems are dynamically self-similar. Whereas the behavior of each system is governed by the same underlying physical mechanisms, the process is amplified to a different extent at each concentration. The logarithmic slope of the collapsed data is approximately 2 for $a_B B \leq 0.2$ T, decreases to approximately 1 (linear dependence) in the range 0.3 T $\leq a_B B \leq 0.6$ T, and subsequently exhibits a plateau. A notable outlier is the data at $\phi_{CIP} = 0.01$ and the highest field strengths, which does not follow quite the same trend as the data for all higher CIP concentrations examined in the present work. Close inspection of this data shows that the field-induced static yield stress for $\phi_{CIP} = 0.01$ does not exhibit a plateau until about $B \geq 0.8$ T (see Fig. 5), as opposed to the plateau observed at about $B \geq 0.6$ T for higher CIP concentrations that corresponds to saturation of the particle magnetization. The reason for this delayed plateau is unclear, but our current hypothesis is that this anomaly is likely an additional result of the

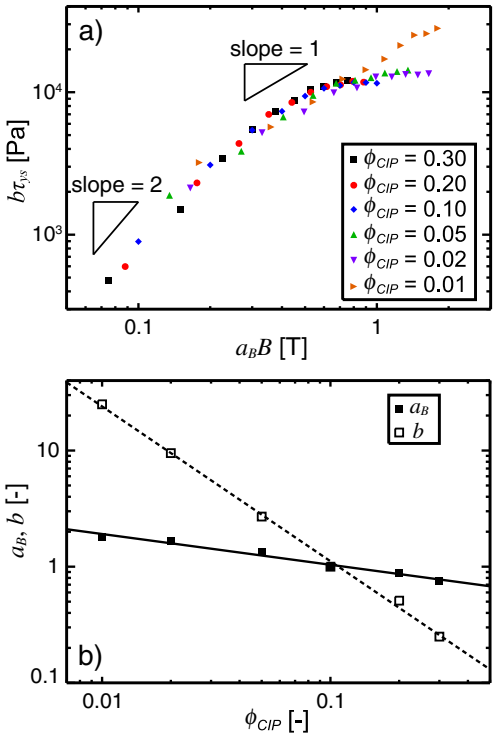

Fig. 7 **a** Master curve showing the reduced field-induced static yield stress as a function of the reduced magnetic field strength in a 3.0 wt% Laponite® matrix fluid at $t_w = 10$ min. Static yield stress measurements for different CIP concentrations are shifted to a reference concentration of $\phi_{CIP} = 0.10$ by the horizontal and vertical shifting factors a_B and b, respectively. As the magnitude of the reduced magnetic field increases, the logarithmic slope of the master curve decreases from 2 to 1 and eventually exhibits a plateau. The only exception is the data at 1 v% CIP, which does not appear to follow the same trend as higher CIP concentrations. **b** Horizontal (a_B) and vertical (b) shift factors for the data presented in (**a**) as a function of the volume fraction of CIP, ϕ_{CIP}. Both sets of shift factors follow a power-law dependence on ϕ_{CIP}; least-squares fitting results in the relationships $a_B \approx 0.56\phi_{CIP}^{-0.26}$ and $b \approx 0.05\phi_{CIP}^{-1.33}$

significant matrix fluid yield stress that hinders chain formation at this dilute CIP concentration for lower magnetic fields (i.e., $Y^*_{M,\phi} \sim 1$), as previously discussed. As the magnetic field is increased, some particles that are restrained by the matrix fluid at lower magnetic fields eventually experience sufficient dipolar forces to overcome the matrix fluid yield stress. This effect may be sensitive to small changes in the average particle magnetization near saturation, but is not expected to be significant for $\phi_{CIP} \geq 0.02$. This behavior could result in the field-induced yield stress exhibiting a plateau at higher applied magnetic fields at $\phi_{CIP} = 0.01$ than for higher CIP concentrations, leading to the poor collapse observed in Fig. 7a.

The variation of the shift factors with the volume fraction of CIP is shown in Fig. 7b. While a_B varies relatively little with ϕ_{CIP}, the vertical shift factor b decreases by about two orders of magnitude from $\phi_{CIP} = 0.01$ to $\phi_{CIP} = 0.30$, reflecting the order of magnitude changes in the field-induced static yield stress over this range of concentrations. That is, τ_{ys} values must be shifted up at low CIP concentrations and down at high CIP concentrations in order to generate the master curve. Both shift factors follow a power-law dependence on ϕ_{CIP} over the range investigated in the present work. Least-squares fitting to a power-law form leads to the expressions $a_B \approx 0.56\phi_{CIP}^{-0.26}$ and $b \approx 0.05\phi_{CIP}^{-1.33}$ $(0.01 \leq \phi_{CIP} \leq 0.30)$. The master curve in Fig. 7, combined with these expressions for the shift factors, can be used to predict the dependence of the field-induced yield stress on the applied magnetic field at CIP concentrations within the range $0.01 \leq \phi_{CIP} \leq 0.30$, and to reasonably extrapolate to higher concentrations.

The master curve in Fig. 7 relates the field-induced yield stress at various CIP concentrations to a macroscopic, externally-set parameter, the applied magnetic field B. Because different types of magnetic particles exhibit different magnetization responses to applied magnetic fields, the behavior shown in Fig. 7 is expected to apply strictly for the particular grade of CIP particles used in the present study. A more general master curve can be developed, however, by considering the dependence of the field-induced yield stress on the average particle magnetization, M, which is an internal variable that characterizes the magnetic response on the particle level (Klingenberg et al. 2007). The magnetization can then be related to the applied field via a magnetization curve, as in Fig. 1c. The characteristic inter-particle magnetic stress, $\tau_{char} = \mu_0 (\rho M)^2 / 24$, which was introduced in Eq. 4, is a physically significant quantity that is set by the average particle magnetization. A correlation or master curve relating the field-induced yield stress and τ_{char} would be applicable for a wide range of magnetic particles because it would be independent of the exact relationship between B and the average particle magnetization, M.

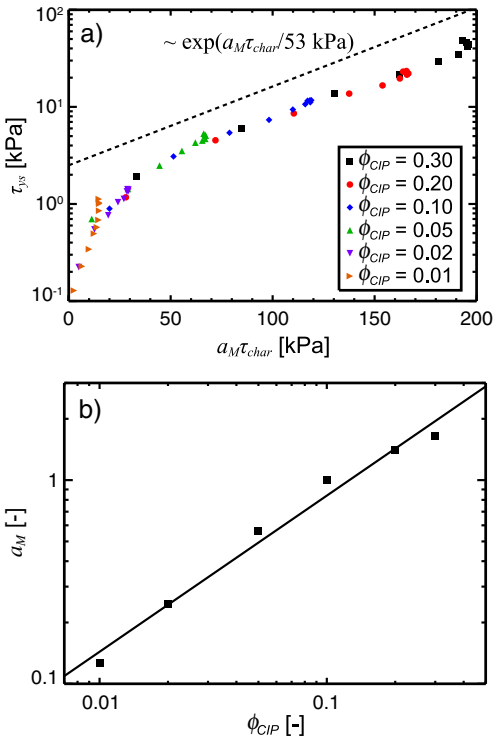

Fig. 8 **a** Alternative master curve for field-induced static yield stress data at various CIP concentrations in a 3.0 wt% Laponite® matrix fluid at $t_w = 10$ min. Here τ_{ys} is plotted as a function of a reduced characteristic magnetic stress between particles, $a_M\tau_{char}$, where a_M is a shift factor and τ_{char} is the characteristic inter-particle magnetic stress given in Eq. 4 that is a function of the average particle magnetization per unit mass, M. Data is again shifted to a reference concentration of $\phi_{CIP} = 0.10$. Since τ_{char} accounts for the magnetization properties of the suspended particulate phase, the above plot is expected to be more generally applicable for different types of magnetic particles than the master curve in Fig. 7a and amounts to a concentration–magnetization superposition. In **b**, the dependence of the shift factor on CIP concentration is shown. A power-law provides a reasonable fit ($R^2 = 0.98$), and least-squares fitting results in the relationship $a_M \approx 4.9\phi_{CIP}^{0.77}$

Figure 8a shows such an alternative master curve relating the field-induced static yield stress to a reduced characteristic inter-particle magnetic stress, $a_M\tau_{char}$, where $a_M(\phi_{CIP})$ is the magnetization–volume fraction shift factor. The fact that shifting is only required on one axis to generate this alternative master curve suggests that the interactions between particles in field-induced chain structures are effectively scaled and characterized by τ_{char} (i.e., by the particle magnetization). As in Fig. 7, yield stress data are again shifted to a reference concentration of $\phi_{CIP} = 0.10$. Data for different values of ϕ_{CIP} are successfully collapsed, once

again with the sole exception of the high magnetic field results for $\phi_{CIP} = 0.01$ as was discussed for the shifting in Fig. 7a. These results effectively amount to a concentration–magnetization superposition. The field-induced static yield stress, τ_{ys}, increases with the magnitude of the reduced characteristic inter-particle stress, exhibiting approximately exponential growth at large values of $a_M \tau_{char}$ (appearing linear on semi-log axes). For $a_M \tau_{char} \geq 30$ kPa the argument of the exponential is about $(53\ \text{kPa})^{-1}$, as shown by the black dotted line. The shift factor a_M increases with the CIP volume fraction, and we show in Fig. 8b that the relationship can be well-approximated as a power-law. Least-squares fitting results in the expression $a_M \approx 4.9\phi_{CIP}^{0.77}$ $(0.01 \leq \phi_{CIP} \leq 0.30)$, where the coefficient of determination is $R^2 = 0.98$. In summary, this alternative master curve for the field-induced static yield stress τ_{ys} in the range $a_M \tau_{char} \geq 30$ kPa can be approximately represented as

$$\tau_{ys} \approx A \exp\left(\frac{a_M \tau_{char}}{\tau^*}\right) \quad (a_M \tau_{char} \geq 30\ \text{kPa}) \tag{8}$$

where $A \approx 1.1$ kPa, a_M is the shift factor given by $a_M \approx 4.9\phi_{CIP}^{0.77}$, $\tau^* \approx 53$ kPa, and τ_{char} is the characteristic inter-particle magnetic stress $\mu_0 (\rho M)^2 / 24$, which is related to the average particle magnetization per unit mass M. This master curve provides a compact expression for design applications in which the magnitude of the yield stress must be predicted for a given field strength, volume fraction, and particle magnetization. The fact that such a master curve can be generated indicates that the field-induced yield stress in these MR fluids arises from a common physical mechanism that acts over a range of conditions, and that this mechanism depends similarly on particle magnetization and concentration. Additionally, the superposition demonstrated in Fig. 8 reinforces the suggestion that higher field-induced yield stresses can be achieved at a given volume fraction by employing particles with a higher saturation magnetization.

Conclusions

The dramatic field-responsive rheological behavior of magnetorheological (MR) fluids, which results from the field-induced chaining of iron microparticles suspended in a matrix fluid, has been successfully employed in the development of numerous field-activated, "smart" soft materials. The stability of MR fluids against particle sedimentation remains an important concern, however, especially in applications where re-dispersion after long off-state times is unfeasible. One proposed solution to this problem is the use of yield stress matrix fluids, and previous authors have investigated the field-induced dynamic yield stress of MR composites in viscoplastic matrix fluids. In the current work, analogous studies of the field-induced *static* yield stress have been performed in MR suspensions in an aging, yield stress matrix fluid. MR composites were formulated from CIP and a matrix fluid consisting of an aqueous dispersion of Laponite® clay, which is known to exhibit a yield stress that grows as the material ages. As a result, sedimentation of CIP is prevented essentially indefinitely. Using a custom-built magnetorheometry fixture, the field-induced static yield stress of this MR composite was studied as a function of the applied magnetic field strength, B, the CIP volume fraction, ϕ_{CIP}, and the age time, t_w. Results were used to generate a magnetorheological master curve (Fig. 8) that indicates a concentration–magnetization superposition and allows prediction of the field-induced yield stress for different types and volume fractions of magnetic particles under a wide range of conditions. A new dimensionless parameter, $\Upsilon^*_{M,\phi}$, was defined (Eq. 6), which relates the magnitude of the matrix fluid yield stress to the characteristic inter-particle magnetic attractive forces at a given particle concentration. For $\Upsilon^*_{M,\phi} \gg 1$, inter-particle magnetic forces dominate and the field-induced rheology is found to be independent of the matrix fluid yield stress. From a practical perspective of MR formulations, this behavior implies that as long as $\Upsilon^*_{M,\phi} \gg 1$, the rheology of the yield stress matrix fluid can be optimized to meet other design demands without significantly disrupting the behavior of the field-activated material. Conveniently, the condition $\Upsilon^*_{M,\phi} \gg 1$ is frequently satisfied at the high field strengths and particle concentrations used in most commercial MR applications.

While the present study has focused solely on shear magnetorheology, the need for quantitative understanding of MR fluids in squeeze flow has recently been highlighted (de Vicente et al. 2011a, b). Because yield stress matrix fluids could play a similar role in preventing particle sedimentation in squeeze flow MR devices, an important question for future work is whether the presence of a matrix fluid yield stress has significant effects on the field-induced squeeze flow rheology of MR composites. An additional interesting problem for future studies would be to focus on some of the anomalies documented in the current work at low volume fractions of magnetic particles. While this dilute regime has limited appeal for traditional MR fluid applications because of the relatively small field-induced yield stresses, the data presented here is suggestive of potentially interesting new regimes and phenomena, which do not appear to have been explored yet. Novel

non-traditional applications could be inspired through an improved understanding of systems at $Y^*_{M,\phi} \sim 1$, for which inter-particle attractive forces are approximately in balance with the matrix fluid yield stress. Numerical simulations could aid in elucidating the dynamics and equilibrium microstructures of dipolar particles under these conditions (Rich et al. 2012).

The results presented here will aid designers of MR devices and guide formulators of MR suspensions in the choice of appropriate viscoplastic matrix fluids. The master curves, correlations, and scaling relationships described in the current study characterize the field-induced static and dynamic yield stress of an MR fluid that is essentially indefinitely stable to sedimentation. This behavior is especially attractive for applications such as active earthquake dampers or field-responsive drilling fluids, for which re-suspension of a dense, concentrated particle phase after long off-state times is typically unfeasible.

Acknowledgements Acknowledgement is made to the Donors of the American Chemical Society Petroleum Research Fund (ACS-PRF Grant No. 49956-ND9) for financial support of this research. The authors are especially grateful to Dr. Murat Ocalan for assistance and many helpful discussions regarding the custom-built magnetorheometry fixture. Further acknowledgement is given to Ki Wan Bong, Dr. Matthew Helgeson, and Dr. Dong Hun Kim for help with SEM imaging, particle size characterization, and Magnetometer measurements, respectively.

References

Abou B, Bonn D, Meunier J (2003) Nonlinear rheology of Laponite suspensions under an external drive. J Rheol 47(4):979–988

Bonn D, Denn MM (2009) Yield stress fluids slowly yield to analysis. Science 324(5933):1401–1402

Bonn D, Kellay H, Tanaka H, Wegdam G, Meunier J (1999) Laponite: what is the difference between a gel and a glass? Langmuir 15(22):7534–7536

Bonn D, Tanase S, Abou B, Tanaka H, Meunier J (2002) Laponite: aging and shear rejuvenation of a colloidal glass. Phys Rev Lett 89(1):015701

Bossis G, Lemaire E (1991) Yield stresses in magnetic suspensions. J Rheol 35(7):1345–1354

Bossis G, Lacis S, Meunier A, Volkova O (2002) Magnetorheological fluids. J Magn Magn Mater 252:224–228

Carlson JD, Matthis W, Toscano JR (2001) Smart prosthetics based on magnetorheological fluids. In: Smart Structures and Materials 2001: Industrial and Commercial Applications of Smart Structures Technologies, vol 4332. Proceedings of the Society of Photo-Optical Instrumentation Engineers (Spie). Spie-Int Soc Optical Engineering, Bellingham, pp 308–316

Chhabra R (1993) Bubbles, drops, and particles in non-Newtonian fluids. CRC, Boca Raton

Chin BD, Park JH, Kwon MH, Park OO (2001) Rheological properties and dispersion stability of magnetorheological (MR) suspensions. Rheol Acta 40(3):211–219

Cho MS, Choi HJ (2004) Magnetorheological characterization of polymer-iron composite suspensions. In: Kang S-G, Kobayashi T (eds) Designing, Processing and Properties of Advanced Engineering Materials, vol 449–452. Materials Science Forum. Trans Tech, Zurich-Uetikon, pp 1201–1204

Cocard S, Tassin JF, Nicolai T (2000) Dynamical mechanical properties of gelling colloidal disks. J Rheol 44(3):585–594

de Vicente J, Lopez-Lopez MT, Gonzalez-Caballero F, Duran JDG (2003) Rheological study of the stabilization of magnetizable colloidal suspensions by addition of silica nanoparticles. J Rheol 47(5):1093–1109

de Vicente J, Vereda F, Segovia-Gutierrez JP, Morales MD, Hidalgo-Alvarez R (2010) Effect of particle shape in magnetorheology. J Rheol 54(6):1337–1362

de Vicente J, Klingenberg DJ, Hidalgo-Alvarez R (2011a) Magnetorheological fluids: a review. Soft Matter 7(7):3701–3710

de Vicente J, Ruiz-Lopez JA, Andablo-Reyes E, Segovia-Gutierrez JP, Hidalgo-Alvarez R (2011b) Squeeze flow magnetorheology. J Rheol 55(4):753–779

Deshmukh SS (2006) Development, characterization and applications of magnetorheological fluid based 'smart' materials on the macro-to-micro scale. Ph.D. Thesis, Dept. of Mechanical Engineering, Massachusetts Institute of Technology, Cambridge, MA, USA

Dyke SJ, Spencer BF, Sain MK, Carlson JD (1996) Modeling and control of magnetorheological dampers for seismic response reduction. Smart Mater Struct 5(5):565–575

Fang FF, Choi HJ, Jhon MS (2009) Magnetorheology of soft magnetic carbonyl iron suspension with single-walled carbon nanotube additive and its yield stress scaling function. Colloid Surface A 351(1–3):46–51

Felt DW, Hagenbuchle M, Liu J, Richard J (1996) Rheology of a magnetorheological fluid. J Intell Mater Syst Struct 7(5):589–593

Fermigier M, Gast AP (1992) Structure evolution in a paramagnetic latex suspension. J Colloid Interface Sci 154(2):522–539

Fielding SM, Sollich P, Cates ME (2000) Aging and rheology in soft materials. J Rheol 44(2):323–369

Ginder JM, Davis LC, Elie LD (1996) Rheology of magnetorheological fluids: models and measurements. Int J Mod Phys B 10(23–24):3293–3303

Goncalves FD, Koo J-H, Ahmadian M (2006) A review of the state of the art in magnetorheological fluid technologies—part I: MR fluid and MR fluid models. Shock Vib Digest 38(3):203–219

Jabbari-Farouji S, Tanaka H, Wegdam GH, Bonn D (2008) Multiple nonergodic disordered states in Laponite suspensions: a phase diagram. Phys Rev E 78(6):061405

Jolly MR, Bender JW, Carlson JD (1999) Properties and applications of commercial magnetorheological fluids. J Intell Mater Syst Struct 10(1):5–13

Joshi YM, Reddy GRK (2008) Aging in a colloidal glass in creep flow: time-stress superposition. Phys Rev E 77(2):021501

Klingenberg DJ (2001) Magnetorheology: applications and challenges. AIChE J 47(2):246–249

Klingenberg DJ, Zukoski CF (1990) Studies on the steady-shear behavior of electrorheological suspensions. Langmuir 6(1):15–24

Klingenberg DJ, Ulicny JC, Golden MA (2007) Mason numbers for magnetorheology. J Rheol 51(5):883–893

Kordonski WI, Golini D (1999) Fundamentals of magnetorheological fluid utilization in high precision finishing. J Intell Mater Syst Struct 10(9):683–689

Kordonski W, Gorodkin S, Zhuravski N (2001) Static field stress in magnetorheological fluid. Int J Mod Phys B 15(6–7):1078–1084

Lemaire E, Meunier A, Bossis G, Liu J, Felt D, Bashtovoi V, Matoussevitch N (1995) Influence of the particle size on the rheology of magnetorheological fluids. J Rheol 39(5):1011–1020

Lim ST, Cho MS, Jang IB, Choi HJ (2004) Magnetorheological characterization of carbonyl iron based suspension stabilized by fumed silica. J Magn Magn Mater 282:170–173

Lim ST, Choi HJ, Jhon MS (2005) Magnetorheological characterization of carbonyl iron–organoclay suspensions. IEEE Trans Magn 41(10):3745–3747

Liu J, Gardel ML, Kroy K, Frey E, Hoffman BD, Crocker JC, Bausch AR, Weitz DA (2006) Microrheology probes length scale dependent rheology. Phys Rev Lett 96(11):118104

Lopez-Lopez MT, de Vicente J, Bossis G, Gonzalez-Caballero F, Duran JDG (2005) Preparation of stable magnetorheological fluids based on extremely bimodal iron-magnetite suspensions. J Mater Res 20(4):874–881

Lopez-Lopez MT, Zugaldia A, Gonzalez-Caballero F, Duran JDG (2006) Sedimentation and redispersion phenomena in iron-based magnetorheological fluids. J Rheol 50(4):543–560

Martin JE, Anderson RA (1996) Chain model of electrorheology. J Chem Phys 104(12):4814–4827

Martin C, Pignon F, Piau J-M, Magnin A, Lindner P, Cabane B (2002) Dissociation of thixotropic clay gels. Phys Rev E 66(2):021401

Møller PCF, Mewis J, Bonn D (2006) Yield stress and thixotropy: on the difficulty of measuring yield stresses in practice. Soft Matter 2(4):274–283

Møller PCF, Fall A, Chikkadi V, Derks D, Bonn D (2009) An attempt to categorize yield stress fluid behaviour. Philos Trans R Soc A-Math Phys Eng Sci 367(1909):5139–5155

Mourchid A, Levitz P (1998) Long-term gelation of Laponite dispersions. Phys Rev E 57(5):R4887–R4890

Mourchid A, Delville A, Lambard J, LeColier E, Levitz P (1995) Phase diagram of colloidal dispersions of anisotropic charged particles: equilibrium properties, structure, and rheology of Laponite suspensions. Langmuir 11(6):1942–1950

Negi AS, Osuji CO (2010) Time-resolved viscoelastic properties during structural arrest and aging of a colloidal glass. Phys Rev E 82(3):031404

Ngatu GT, Wereley NM, Karli JO, Bell RC (2008) Dimorphic magnetorheological fluids: exploiting partial substitution of microspheres by nanowires. Smart Mater Struct 17(4):8

Nguyen QD, Boger DV (1992) Measuring the flow properties of yield stress fluids. Annu Rev Fluid Mech 24:47–88

Ocalan M (2011) Magnetorheological fluids for extreme environments: stronger, lighter, hotter. Ph.D. Thesis, Dept. of Mechanical Engineering, Massachusetts Institute of Technology, Cambridge, MA, USA

Olabi AG, Grunwald A (2007) Design and application of magneto-rheological fluid. Mater Design 28(10):2658–2664

Park JH, Kwon MH, Park OO (2001) Rheological properties and stability of magnetorheological fluids using viscoelastic medium and nanoadditives. Korean J Chem Eng 18(5):580–585

Park BJ, Fang FF, Choi HJ (2010) Magnetorheology: materials and application. Soft Matter 6(21):5246–5253

Park BO, Park BJ, Hato MJ, Choi HJ (2011) Soft magnetic carbonyl iron microsphere dispersed in grease and its rheological characteristics under magnetic field. Colloid Polym Sci 289(4):381–386

Parthasarathy M, Klingenberg DJ (1996) Electrorheology: mechanisms and models. Mat Sci Eng R 17(2):57–103

Petit L, Barentin C, Colombani J, Ybert C, Bocquet L (2009) Size dependence of tracer diffusion in a Laponite colloidal gel. Langmuir 25(20):12048–12055

Phulé PP, Mihalcin MP, Genc S (1999) The role of the dispersed-phase remnant magnetization on the redispersibility of magnetorheological fluids. J Mater Res 14(7):3037–3041

Rabinow J (1948) The magnetic fluid clutch. AIEE Trans 67:1308–1315

Rankin PJ, Horvath AT, Klingenberg DJ (1999) Magnetorheology in viscoplastic media. Rheol Acta 38(5):471–477

Rich JP, Lammerding J, McKinley GH, Doyle PS (2011a) Nonlinear microrheology of an aging, yield stress fluid using magnetic tweezers. Soft Matter 7(21):9933–9943

Rich JP, McKinley GH, Doyle PS (2011b) Size dependence of microprobe dynamics during gelation of a discotic colloidal clay. J Rheol 55(2):273–299

Rich JP, McKinley GH, Doyle PS (2012) Arrested chain growth during magnetic directed particle assembly in yield stress matrix fluids. Langmuir 28(7):3683–3689

Ruzicka B, Zaccarelli E (2011) A fresh look at the Laponite phase diagram. Soft Matter 7(4):1268–1286

Ruzicka B, Zulian L, Ruocco G (2004) Routes to gelation in a clay suspension. Phys Rev Lett 93(25):258301

Ruzicka B, Zulian L, Ruocco G (2006) More on the phase diagram of Laponite. Langmuir 22(3):1106–1111

Shahin A, Joshi YM (2010) Irreversible aging dynamics and generic phase behavior of aqueous suspensions of laponite. Langmuir 26(6):4219–4225

Spencer BF, Dyke SJ, Sain MK, Carlson JD (1997) Phenomenological model for magnetorheological dampers. J Eng Mech-ASCE 123(3):230–238

Thompson DW, Butterworth JT (1992) The nature of Laponite and its aqueous dispersions. J Colloid Interface Sci 151(1):236–243

Volkova O, Bossis G, Guyot M, Bashtovoi V, Reks A (2001) Magnetorheology of magnetic holes compared to magnetic particles. J Rheol 44(1):91–104

Waigh TA (2005) Microrheology of complex fluids. Rep Prog Phys 68(3):685–742

Zhang K, Choi BI, Choi HJ, Jhon MS (2010) Comment on 'Fabrication of uniform core-shell structural calcium and titanium precipitation particles and enhanced electrorheological activities'. Nanotechnology 21(37):378001

Zitha PLJ (2004) Method of drilling with magnetorheological fluid. US patent number 7021406